Journal of Aerosol Science 76 (2014) 163–174

Contents lists available at ScienceDirect

Journal of Aerosol Science

journal homepage: www.elsevier.com/locate/jaerosci

Maximal efficiency of convective mixing occurs in mid acinus: A 3D-numerical analysis by an Eulerian approach

Pierre-Antoine Muller [a,b], Marine Pichelin [a], Gabriela Apiou [b], Bruno Louis [b], Ira Katz [a,c], Georges Caillibotte [a], Marcel Filoche [b,d], Daniel Isabey [b,*]

[a] Medical R&D of Air Liquide Healthcare, Centre de Recherche Paris-Saclay, Jouy-en-Josas, France
[b] Inserm, U955 (Equipe 13) and CNRS ERL 7240, Cell and Respiratory Biomechanics, Université Paris Est, Créteil, France
[c] Department of Mechanical Engineering, Lafayette College, Easton, PA, USA
[d] Physique de la Matière Condensée, Ecole Polytechnique, CNRS, 91128 Palaiseau, France

ARTICLE INFO

Article history:
Received 19 March 2014
Received in revised form
11 June 2014
Accepted 12 June 2014
Available online 2 July 2014

Keywords:
Computational fluid dynamics (CFD)
Acinar flow
Alveoli
Deforming wall
Alveolar clearance

ABSTRACT

Despite very low Reynolds numbers in the bronchial ducts, acinar flow associated with wall motion can exhibit irreversibility and chaoticity, two efficient features of convective mixing contributing to alveolar dispersion. This paper describes a new computational fluid dynamics (CFD) approach in which an Eulerian continuous scalar field transported by fluid flow is used as a numerical tracer to quantify convective mixing in an incompressible flow of non-diffusive fluid. This flow cyclically enters into and exits from an elementary alveolar model made of a single beating alveolus connected to a deformable bronchiole. A non-dimensional parameter defined as the residual mass of marked fluid normalized by the initial alveolar mass of fluid, m_{res}, is used to study the efficiency of convective mixing in different conditions of alveolar ventilation. This parameter is dependent on the alveolar-to-bronchial flow ratio, Q_A/Q_D, which reveals that a relative maximum efficiency for convective mixing is expected to occur in the mid acinar region in quasi-normal conditions of breathing.

1. Introduction

Despite very low Reynolds numbers in the lumen of alveolar ducts, acinar flow can exhibit irreversibility in the alveoli due to the wall motion as first demonstrated by Tsuda et al. (1995) using numerical simulations. Following this work, several more numerical and experimental studies (Chhabra & Prasad, 2010; Haber et al., 2000; Henry et al., 2002; Kumar et al., 2009; Tsuda et al., 1999, 2008) have confirmed that the flow in the alveolar region is often kinematically irreversible and chaotic — more specifically, that a fluid particle entering an alveolus during inhalation would not follow the same pathway during exhalation. This flow irreversibility can also affect aerosol particles (Darquenne et al., 2009; Haber et al., 2003; Tsuda et al., 2008) because fine particle transport in the alveoli includes a convective component in addition to a diffusive component. In this regard it has been shown that particle deposition in alveoli is a function of residence time (Darquenne et al., 2009) that in turn is influenced by the irreversible flow effects (Chhabra & Prasad, 2010; Darquenne et al., 2009; Lee & Lee, 2003; Tippe & Tsuda, 2000). However, quantifying the amount of mixing often requires

* Corresponding author.
E-mail address: daniel.isabey@inserm.fr (D. Isabey).

http://dx.doi.org/10.1016/j.jaerosci.2014.06.006
0021-8502/

computing the trajectories of a large number of particles, large enough to explore the various chaotic evolutions of a fluid volume initially located in the duct.

This paper describes an alternative computational fluid dynamics (CFD) model of alveolar flow in a single alveolus connected to a bronchiole duct that uses an Eulerian approach to account for alveolar mixing. Specifically, a fluid material volume initially in the duct is marked. Through the breathing cycle for one or more breaths the amount of marker that enters the alveolus is used as a measure of the extent of alveolar flow mixing. This mixing is assumed to correlate with flow irreversibility and chaoticity initially discovered by previous authors (Tsuda et al., 1999, 2008). The end goal is to use this measure as the basis of a compact analytical form to quantify flow mixing as a function of physiological and ventilatory parameters that could be employed in a particle deposition model.

2. Methods

2.1. Geometrical model

The geometrical model used herein is composed of a single alveolar cavity connected to a respiratory bronchiole (duct) (see Fig. 1) whose characteristic dimensions are given for nominal values in Table 1.

2.2. Wall deformation and flow conditions

There is no consensus in the literature about the homogeneity of lung tissue deformation (Forrest, 1970; Greaves et al., 1986; Kitaoka et al., 2007). However, new imaging techniques hold some promise of determining alveolar wall motion

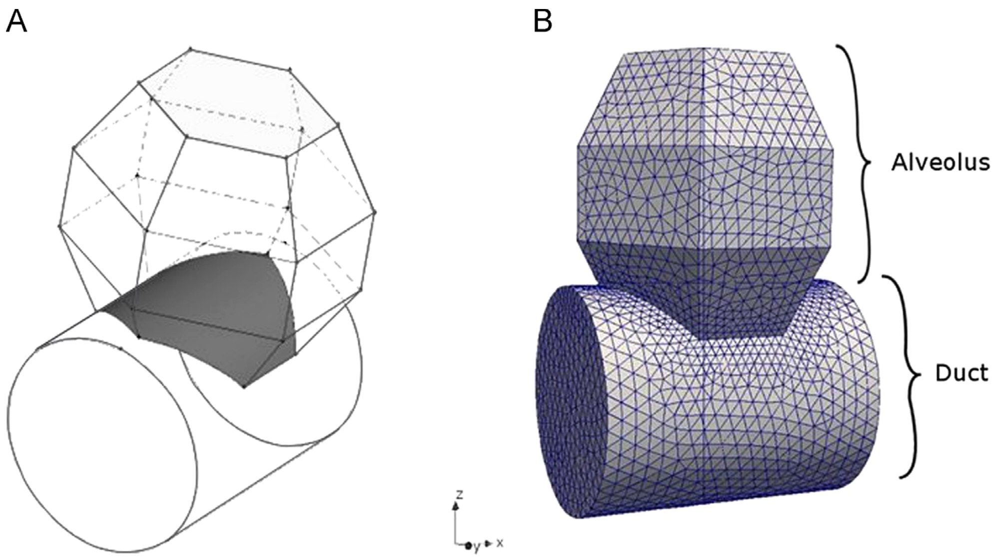

Fig. 1. Geometry (A) and CFD mesh (B) of the alveolus model. The shape of the alveolus is a 19 face polyhedron, constituted of a stack of four connected hexagonal cross sections. This shape is consistent with images from histological slices that depict a polygonal (non-spherical) structure of the alveolus, and with the observations of Butler et al. (1996) that the average angle between alveolar septa is 120°. The alveolus is connected to a cylindrical tube representing the respiratory bronchiole through a duct–alveolar interface. The nominal dimensions of these elements are based on morphometric measurements made on human acini (Haefeli-Bleuer & Weibel, 1988; Sznitman et al., 2007; Weibel et al., 2005). Characteristic dimensions of the alveolus model are given in Table 1.

Table 1
Characteristic dimensions of the geometrical model defined by its nominal values.

Characteristic dimensions		
Alveolus	Volume	2.06×10^{-2} mm^3
	Diameter	0.34 mm
Duct	Volume	2.2×10^{-2} mm^3
	Diameter	0.28 mm
	Length	0.356 mm
Duct–alveolus interface	Surface area	5.17×10^{-2} mm^2

(Unglert et al., 2010). Within the chest, alveolar tissues rhythmically deform during breathing under the effect of diaphragm and ribcage motion. The resulting motion of the parenchyma is modeled in our simulation as an isotropic, time-dependent transformation of the entire model geometry that is a function of the breathing parameters (lung volumes and breathing period).

The amplitude of the deformation is considered proportional to the deformation of the whole lung and thus assumes a uniform lung deformation. Therefore, the volume based coefficient of similarity $H(t)$ is defined by

$$H(t) = \frac{V_{geom}(t)}{V_{geom}(FRC)} \tag{1}$$

where $V_{geom}(t)$ is the volume of the calculation domain which includes the alveolus and the duct at a given time t and $V_{geom}(FRC)$ is the volume of the domain when the lung is at the functional residual capacity (FRC) – the volume at the beginning of inhalation. Assuming a sinusoidal breathing pattern the length-scale coefficient used for isotropic deformation $h(t)$ is defined as

$$h(t) = H(t)^{1/3} = \left(1 + \frac{V_T}{V_{FRC}}\left[\frac{1}{2} - \frac{1}{2}\cos\left(2\pi\frac{t}{T}\right)\right]\right)^{1/3} \tag{2}$$

where V_T is the tidal volume, V_{FRC} is the FRC of the lung, and T is the breathing period (see Fig. 2A for a representation of the evolution of $h(t)$). Amplitude and frequency of the wall motion are functions of the breathing parameters; e.g., pulmonary volumes or breathing period through Eq. (2). Thereby, the variations of the acinus are assumed to remain proportional to the variations of the whole chest volume suggesting a uniform deformation of homothetic nature for lung tissues. A consequence is that sizes of both the alveolus and the duct change proportional to this length-scale coefficient while these changes remain in phase during a whole breathing cycle in the acinar model.

The flow rate in the duct, Q_D, is also assumed to be sinusoidal and always in-phase with geometrical deformation. Q_A represents the flow rate entering into or exiting from the alveolus during the inhalation phase or the exhalation phase (see Fig. 2B). The chaotic behavior of the flow has been shown to arise in such a rhythmically expanding/contracting alveolus (Tsuda et al., 1995) when the creeping oscillatory recirculation flow is perturbed by a low level of convective inertia effects such as those corresponding to maximum Reynolds number as low as 0.5 and below (see Table 2).

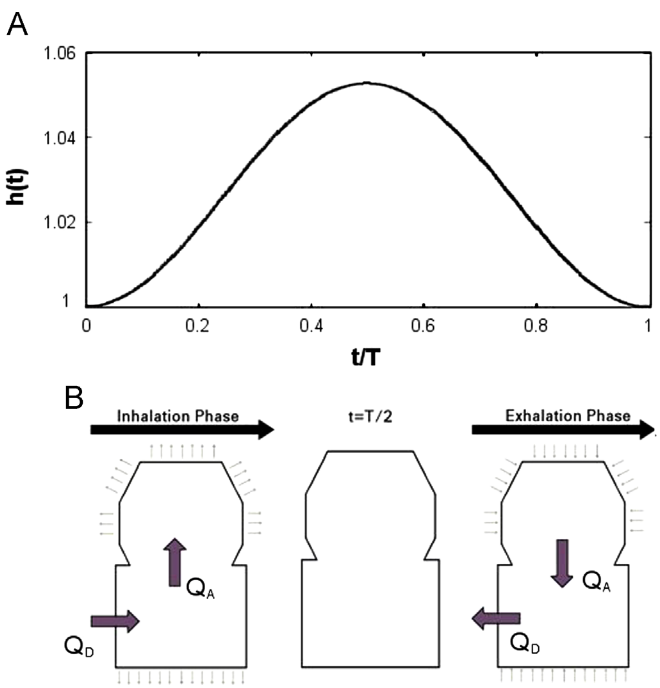

Fig. 2. Illustration of the wall deformation and flow conditions in the numerical model. Panel A: Sinusoidal evolution of the length-scale coefficient $h(t)$ as a function of time. At $t/T = 0.5$, the deformation is at the maximal level of about 5% (in length). Panel B: In phase evolution of the geometry during the breathing cycle: expansion of the duct and the alveolus during inhalation (from $t=0$ to $t=T/2$) and contraction during exhalation (from $t=T/2$ to $t=T$). Q_A represents the flow rate entering/exiting the alveolus; Q_D is the flow rate in the duct directly above the inlet of the alveolus. These two flow components are in phase with the geometrical deformations. The maximal deformation is observed at $t=T/2$.

Table 2
Non-dimensional numbers characteristic of the flow. Reynolds number ($Re=UD/\nu$), Strouhal number ($St=D/TU$), Stokes number ($Stk=\rho_p d_p^2 UC_c/18\mu D$), and Péclet number ($Pe=UD/\mathcal{D}_{Brown}$), where U is the characteristic velocity in the duct, D is the duct diameter, T is the breathing period, ρ_p and d_p are the density and diameter of the particles, μ is the gas dynamic viscosity, and C_c is the slip correction factor as defined by Hinds (2014), $\mathcal{D}_{Brown}$ is the coefficient of Brownian diffusion and ν is the gas kinematic viscosity. Estimation using the Weibel (1963) lung model for V_T=0.5 L and T=3 s. The range of values corresponds to the evolution of these dimensionless numbers throughout the acinar region.

Reynolds number	5×10^{-3}–0.5
Strouhal number	10^{-2}–0.7
Q_A/Q_D	5×10^{-3}–5×10^{-1}
Stokes number (0.1–1 μm particle)	10^{-7}–10^{-4}
Particle Péclet number (0.1–1 μm particle)	5×10^{3}–10^{3}

2.3. Distribution of Q_A/Q_D in the lung model

The ratio Q_A/Q_D has been considered in several studies as characterizing alveolar flow (see Sections 3 and 4). The deformation controls the value of the flow rate penetrating the alveolar cavity (Q_A) at each cycle:

$$Q_A(t)=\dot{H}(t)V_A(FRC) \tag{3}$$

where $\dot{H}(t)$ is the time-derivative of the volume-coefficient of similarity (see Eq. (1)) and $V_A(FRC)$ is the volume of the alveolar cavity at the beginning of the inhalation phase. Based on a symmetric lung morphometry model (Soong et al., 1979), Q_D can be estimated in a given acinar generation (the index g) by calculating the volume variation of the acinar region subtended by a given acinar generation:

$$Q_D(t)=\dot{H}(t)\left[\sum_{k>g}2^{k-g}V_k+\frac{V_g}{2}\right] \tag{4}$$

where V_k is the volume of one segment, in generation k (alveoli and bronchiole), assuming that each generation is constituted of segments. Following Eq. (4), the deeper the alveolar position g, the weaker the flow rate in the duct Q_D. This consequence of the airway branching geometry results in an increase in the ratio Q_A/Q_D as the generation number increases. Based on this analysis, note that this ratio is not a function of the ventilatory parameters.

2.4. Numerical method

Dimensionless numbers can be calculated to illustrate the main characteristics of the fluid dynamics of this system. The Reynolds number and the Strouhal number, which are the key dimensionless parameters that characterize the duct flow, have been calculated using physiologically relevant parameters (see Table 2). The former measures the influence of convective inertia compared to viscous effects, whereas the latter characterizes the relative contributions of the oscillating and steady flows in terms of local to convective inertia ratio. In our case, the Reynolds number range corresponds to a laminar viscous dominated flow throughout the acinus. Strouhal number values are lower than one, indicating that unsteady effects are negligible because local gas inertia is low compared to convective inertia. However, the alveolar wall motion (implemented via time-dependent boundary conditions) is not accounted for in these duct based parameters. The Stokes and Péclet numbers for aerosol particles will be considered in Section 4.

CFD calculations of the three-dimensional, incompressible Navier–Stokes equations were performed to determine the flow fields in the alveolus model using the commercial software Fluent™ (ANSYS, PA, USA). Grid transformation is performed at each time step by a user defined function (following Eq. (2)) to adjust positions of the alveolar wall mesh nodes which define the moving boundary. The other boundary conditions are as follows: (i) no-slip boundary condition at the walls, (ii) pressure boundary condition at the inlet (proximal opening of the duct), and (iii) a mass flow outlet at the distal open end of the duct. A sinusoidal time dependent outlet mass flow condition was implemented using a user defined function, in phase with the geometrical deformation. This scheme therefore conserves mass. Its amplitude is in the physiological range of values taken by Q_D (see Eq. (4)) in all the generations of the acinus. An unstructured three-dimensional mesh was created with Gambit software (ANSYS, PA, USA). Grid convergence tests were performed based on axial and lateral velocity profiles in the geometry.

2.5. Tracking the fluid material volume: residual mass

CFD simulations yield the time-dependent velocity field at all points in the model geometry. However, this Eulerian description of the flow at spatial locations does not readily provide a measure for the flow irreversibility. To this end, typically a Lagrangian approach is used where the motions of individual fluid particles are tracked through numerical integration of their trajectories in the oscillating flow field. The flow chaoticity and irreversibility can then be measured using the time behavior of averaged distances between particles. We have chosen here an alternative approach that consists in computing the evolution of an Eulerian continuous scalar field transported by the fluid flow. This field denoted ϕ acts as a marking of the fluid particles, i.e., as a “numerical tracer”. Because it does not affect the fluid flow it is called a “passive scalar". This field is initially set to 1 in the bronchiole duct and to 0 in the alveolus, therefore marking the material fluid volume that is initially in the bronchiole duct and that enters the alveolar space during the inhalation phase of the first breathing cycle. This numerical approach is equivalent to physically marking the fluid with smoke or dye; however, ϕ is non-diffusive as compared to the physical flow visualization methods, which allows us to directly assess the efficiency of the mixing in the convective transport, something usually difficult to achieve experimentally. The local (mass conservation) transport equation for ϕ is given by

$$\frac{\partial(\rho\phi)}{\partial t}+\text{div}\left(\rho\phi\vec{V}\right)=0 \tag{5}$$

where ρ is the density of the fluid (presently assumed to be constant) and $\vec{V}$ is the fluid velocity. Initial scalar values are $\phi=0$ (0% scalar concentration) in the alveolus and $\phi=1$ (100% scalar concentration) in the duct (seen at t=0). Boundary conditions for the scalar are

$$\begin{cases} \phi=1 & \text{at the inlet surface} \\ \dfrac{d\phi}{dx}=0 & \text{at the outlet surface} \end{cases} \quad \text{during inhalation,} \quad t<T/2 \tag{6}$$

and

$$\begin{cases} \phi=0 & \text{at the inlet surface} \\ \dfrac{d\phi}{dx}=0 & \text{at the outlet surface} \end{cases} \quad \text{during exhalation,} \quad T/2<t<T \tag{7}$$

Note that the inlet and outlet surfaces are inverted for exhalation compared to inhalation. After the first breathing cycle, $\phi=0$ at the inlet surface during inhalation. The transport equation (see Eq. (5)) is solved using a User Defined Scalar function without the diffusion option, implemented within FLUENT. One has to note that, since there is no diffusive term in the transport equation (5), the evolution of a field initially piecewise constant on two separate regions (Fig. 3a) should result at later times in a still piecewise constant field on two separate new regions (Fig. 3b). The boundary between the new regions results from the evolution of the initial separation line between the duct and the alveolus in the unsteady velocity field (upper thick arrow between Fig. 3a and b). Theoretically, if the flow field in the second half-period of the breathing is the time-reversed field of the first half-period (which would be the case for a Stokes flow since the motion of the walls is symmetric in time), then the separation line should come back to its initial position (lower thick arrow in Fig. 3).

The origin of the irreversibility observed in our numerical simulations is mainly the convective inertia component of the flow which causes the flow field in the second half-period of the breathing to differ from the time-reversal of the one in the first half. Incidentally, the artificial diffusion coming from the discretization scheme and the numerical simulation will smooth the step-wise distribution of the passive scalar (ϕ) and spread it into the alveolus in addition to the convective and chaotic mixing reported above. However, due to the good spatial convergence (Roache, 1982) and previous testing of the Fluent User Defined Scalar function in the literature (Glatzel et al., 2008) the effect of artificial diffusion is insignificant. The field ϕ thus provides a natural measure of convective mixing efficiency of the fluid during the breathing cycle. Moreover, it is expressed in an Eulerian scheme which makes it very easy to implement in a numerical simulation and to solve with the known velocity field at each step. By observing the residual amount of fluid mass marked by the scalar in the alveolar cavity after a limited number of breathing cycles, we can obtain a compact quantification of the flow irreversibility. The amount of marked fluid remaining after n cycles ($m_{res}(n)$) is calculated by integrating the passive scalar $\phi(\vec{x},t)$ over the alveolus at

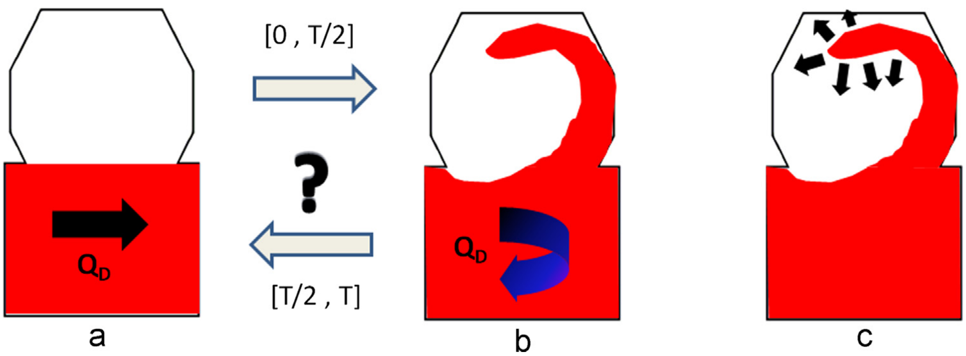

Fig. 3. Theoretical evolution of the passive scalar field ϕ during a single breath. (a) Initial value of the field which is set to 1 in the acinar duct and to 0 in the alveolus. The flow runs from left to right. (b) Being carried by the fluid, the field ϕ should remain a step-wise function throughout its evolution. If the flow field in the second half-period is the time-reversed of that in the first half-period, then the distribution of ϕ should return to its initial value at the end of the period. (c) In fact, flow asymmetry in time and chaoticity of the flow combine to produce an irreversible dispersion of the field ϕ, making it an effective tool to measure the irreversibility of the system.

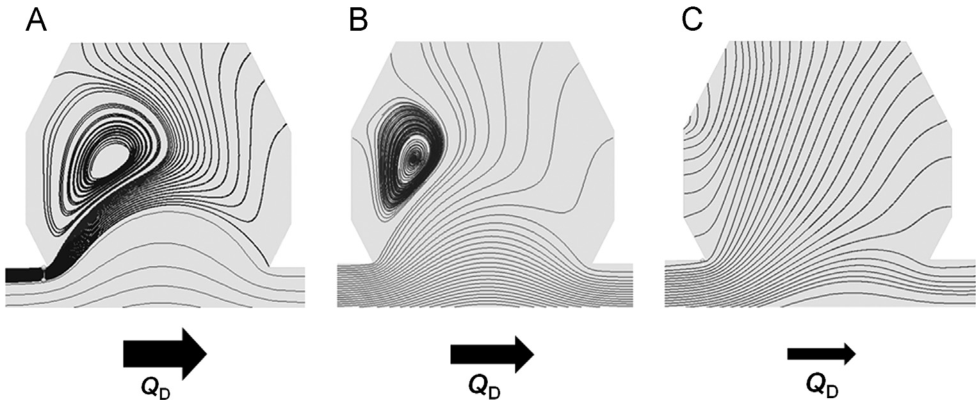

Fig. 4. Instantaneous flow patterns at peak inspiration obtained for different alveolar-to-bronchial flow ratio values. The flow runs from left to right. Streamlines are calculated in the central plane using the current numerical model. (A) $Q_A/Q_D = 0.008$; (B) $Q_A/Q_D = 0.016$; and (C) $Q_A/Q_D = 0.15$.

time $t=nT$, and normalizing it by the volume of fluid in the alveolus ($V_A(FRC)$) at the beginning of inhalation:

$$m_{res}(n) = \frac{\iiint_{alv} \phi(\vec{x}, t)\, d^3x}{\iiint_{alv} 1 \cdot d^3x} = \frac{\iiint_{alv} \phi(\vec{x}, t)\, d^3x}{V_A(FRC)} \tag{8}$$

$m_{res}(n)$ provides a non-dimensional estimate of the balanced effect between marker penetration (during alveolar inflation) and marker washout (during alveolar deflation) over one or several (n) entire cycles of alveolar filling and emptying. The computational implementation of $m_{res}(n)$ was accomplished by the integration of flux of the marker across the surface between the duct and the alveolus at each time step. This surface integral can be shown to be equivalent to the volume integral in Eq. (8).

3. Results

The instantaneous flow patterns calculated at peak inspiration (shown in Fig. 4) in the present 3D-model are quite similar to those obtained in the 2D-model by Tsuda et al. (1995). The latter results were obtained under the same flow conditions but for a slightly different moving walls acinar model. Minor changes in the geometrical shape of the alveolus did not affect the key features of the flow fields.

Large recirculation zones were observed for very low values of Q_A/Q_D ($Q_A/Q_D = 0.008$) but not for larger values ($Q_A/Q_D = 0.15$) where radial streamlines are visible. The occurrence of a recirculation zone at small values of Q_A/Q_D has also been obtained in previous numerical models (Kumar et al., 2009; Sznitman et al., 2009) and experimental studies (Tippe & Tsuda, 2000). Such alveolar flow patterns obtained in certain conditions of alveolar wall motion and flow pattern are known to promote kinematic irreversibility of fluid particles, initiation of a stagnation saddle point and the existence of chaotic alveolar flow behavior (Henry et al., 2009). It implies that a fluid particle might not follow the same path during inhalation and during exhalation even though conditions of the calculation are reversible in terms of wall motion and flow boundary conditions.

3.1. Single breath analysis

Figure 5 presents the dispersion of the tracer in the acinar model at five different instants during the first breathing cycle. The distribution of the passive scalar can be visualized in the whole domain (duct and alveolus) at each time-step of the 3D numerical computation. Colors indicate the repartition of scalar values, where black corresponds to a scalar value of 0 and red is 1, indicating that all the fluid in a given volume was not or was from the originally marked bolus, respectively.

The images shown in the top part of Fig. 5 are not 2D slices but 3D representations of the numerical domain using modified transparency values to obtain a blended superposition of all data contained in the successive slices of the domain. Fig. 5 provides a qualitative illustration of the evolution of the passive scalar field during the first complete breathing cycle. For this example, Q_A/Q_D value is 7×10^{-4} and exhibits irreversible flow recirculation. This is expected for such low Q_A/Q_D values as indicated by Fig. 4 and reported in the literature (Tsuda et al., 1995). The effect of kinematic irreversibility of alveolar flow is clearly visible on the evolution of numerical tracer first by comparing instants (i.e., $T/4$ and $3T/4$) where alveolar flows have the same magnitude but opposite directions.

Second, at the end of the first breathing cycle, the alveolus is no longer free of tracer, indicating that some marked fluid originally in the duct remains located in the alveolus in spite of total reversibility of duct and alveolar wall motion. These results are consistent with a rapid dispersion of the numerical scalar which occurs within less than one breath, suggesting that non-reversibility of fluid particle motion and the chaotic behavior of alveolar flow generate a very efficient convective

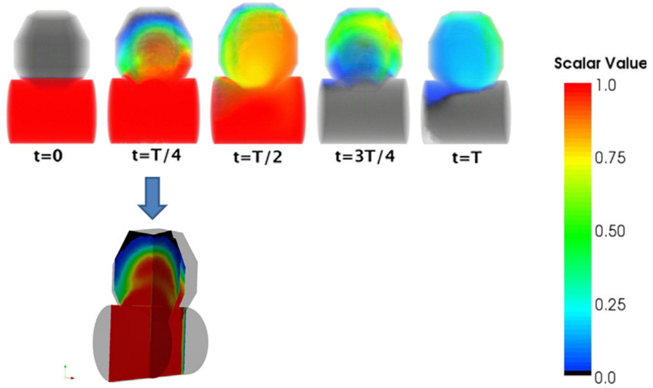

Fig. 5. (Top) Evolution of the passive scalar values according to a 3D-representation. Scale indicates the scalar value (from 0 to 1) or concentration (from 0% to 100%) at different characteristic times during the first breathing cycle. As in Figs. 3 and 4, the duct flow runs from left to right. (Bottom) The cross-sectional representation of scalar value (or concentration) in the axial and perpendicular planes of the model at $t=T/4$. The overall breathing conditions are: $Q_A/Q_D=7\times10^{-4}$, $T=3$ s, V_T=0.5 L, V_{FRC}=3 L. The value used for Q_A/Q_D corresponds to a proximal position in the acinar tree.

mixing that can be advantageously quantified by the normalized amount of residual scalar remaining in the alveolar cavity at the end of each breathing cycle.

Values of m_{res} are plotted in Fig. 6 as a function of Q_A/Q_D and for a physiological range of these values, i.e., from 3×10^{-4} to 10^{-1}, calculated on the basis of Eq. (4) and the geometrical values of the morphometric model by Soong et al. (1979). These values cover a complete range of positions in the acinus, i.e., generations 17–23, and the present results reveal maximum mixing efficiency for the intermediate acinus generations.

Regarding the top curve obtained after the first breathing cycle, low values are obtained near the two extremities of the range (10^{-4}–10^{-1}) for Q_A/Q_D. It suggests that low convective mixing occurs in both the more distal and the more proximal regions of the acinus. As a matter of fact, in the distal part of the acinus, flow might be more reversible first because *Re* takes the lowest values there, and second because at higher values of Q_A/Q_D the recirculating zone in the alveolar cavity progressively vanishes, as displayed in Fig. 4C. For the proximal part of the acinar compartment, the dominating duct flow limits transport of scalar into the alveolar cavity, thus isolating the effect of the alveolar wall motion from fluid in the duct. Thus, the most striking aspect of the curve shown in Fig. 6 is the maximum that occurs near $Q_A/Q_D=2.5\times10^{-3}$ corresponding to the middle range of acinar generations, i.e., 20–21. Here the interaction between the alveolar flow and the duct flow is the largest, resulting in the greatest flow irreversibility and chaoticity. The washout resulting from the succession of alveolar breathing cycles (up to 9) consistently confirms that an efficient convective mixing mechanism enables a rapid decrease in the normalized amount of residual scalar.

3.2. Multi-breath analysis

The multi-breath analysis shown in Figs. 7 and 8 describes the decay in residual scalar remaining after the first cycle and removed by several successive alveolar breathing maneuvers free of new marker. Because no new passive scalar is introduced after the first cycle, these calculations over several breathing cycles provide a quantification of the multi-breath alveolar washout and its modulation through the acinar region. Figure 7 displays the dispersion of the scalar bolus in the alveolus during the first cycle (1*T*) followed by five successive breathing cycles (from 2 to 6 cycles) for the case $Q_A/Q_D=7\times10^{-4}$ corresponding to proximal acinar generation (#17–18). As shown in Fig. 6, m_{res} is drastically reduced by washout from the alveolus dependent on the position in the acinus.

To illustrate how acinar position may affect the washout rate, m_{res} was plotted in Fig. 8 as a function of breathing cycle for three physiological values of Q_A/Q_D ranging from proximal to distal acinar regions. When Q_A/Q_D is low (3×10^{-4}), i.e., in the proximal acinar regions, the flow velocity entering the alveolus is small compared to the shear flow generated by duct flow thus justifying the small values observed at the end of the first inhalation (see Fig. 8A). When Q_A/Q_D is high (1.1×10^{-1}), the shear imposed by the flow in the duct is weak and the dominant effect is the aspiration of marked fluid into the alveolar cavity; however, m_{res} at the end of the first inhalation is now low due to the highly reversible nature of the flow (see Fig. 8C) which also explains why the trapped marked fluid does not washout during the following breathing cycles. The case $Q_A/Q_D=2.5\times10^{-3}$ corresponds to the maximum value of m_{res}, where shear and aspiration mechanisms are balanced, leading to a high uptake and retention of marked fluid into the alveolus and slow washout (Fig. 3b).

3.3. Output of the model

The output of the model is exemplified in Fig. 8 where m_{res} is plotted as a function of the number of unloaded breathing cycles (up to 9) following a first loaded cycle and three different values of Q_A/Q_D corresponding approximately to

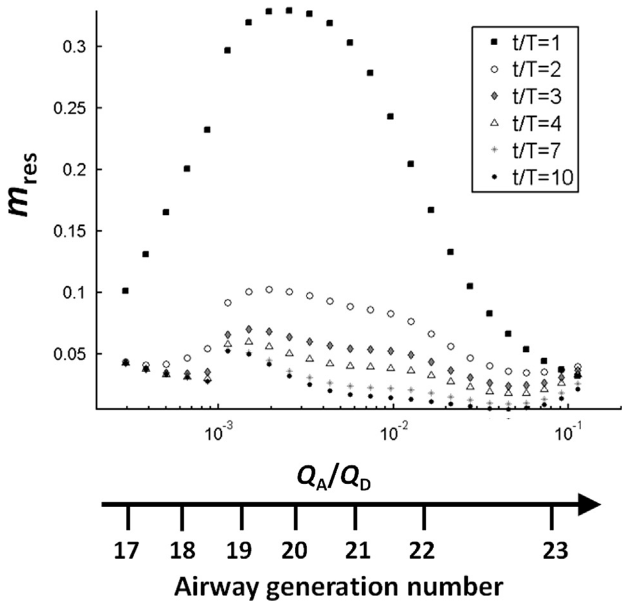

Fig. 6. Calculated impact of alveolar-to-duct flow ratio Q_A/Q_D on the normalized amount of residual scalar remaining in the alveolar cavity at the end of 1 breathing cycle (in proportion of the initial quantity of scalar in the alveolus of the model) and its washout resulting from a succession of cycles (up to 9 after the first loaded cycle). The values of Q_A/Q_D represent different airway generations indicated by a second horizontal axis based on data by Soong et al. (1979).

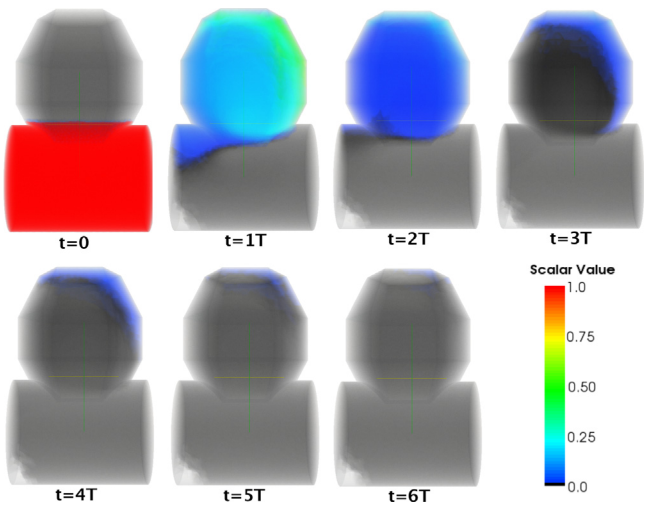

Fig. 7. Simulation of a washout maneuver of the marked fluid after 1 loaded cycle of marker followed by five unloaded breathing cycles (the duct flow runs from left to right). The physiological conditions are $Q_A/Q_D=7\times10^{-4}$, $T=3$ s, $V_T=0.5$ L, $V_{FRC}=3$ L.

proximal (A), intermediate (B) and distal (C) acinar airway generations. This model output can be fitted with an analytical form for later use as part of an aerosol deposition model (Pichelin et al., 2012). Assuming washout can be characterized by an exponential decay, two distinct time scales emerge. Because we are only considering 10 cycles, the long time scale can be realized simply as an additive constant, noted m_T in Eq. (9). The short exponential time scale is characterized by a time constant and the initial (after the first loaded cycle) amount of the numerical tracer in the alveolus, τ and m_I, respectively. The resulting analytical expression is

$$m_{res}(n)=m_I\exp\left(-\frac{n-1}{\tau}\right)+m_T \tag{9}$$

where n is an integer from 1 to 10 representing the loaded cycle and nine successive unloaded cycles.

For example, τ, m_I and m_T, for the Q_A/Q_D values and their associated generation number of the Soong model (Soong et al., 1979), are given in Table 3. The m_I values reflect the relative maximum of convective mixing efficiency at generation 20 (mid acinar region). However, τ increases moving deeper in the acinus and m_T shows a relative maximum at generation 19.

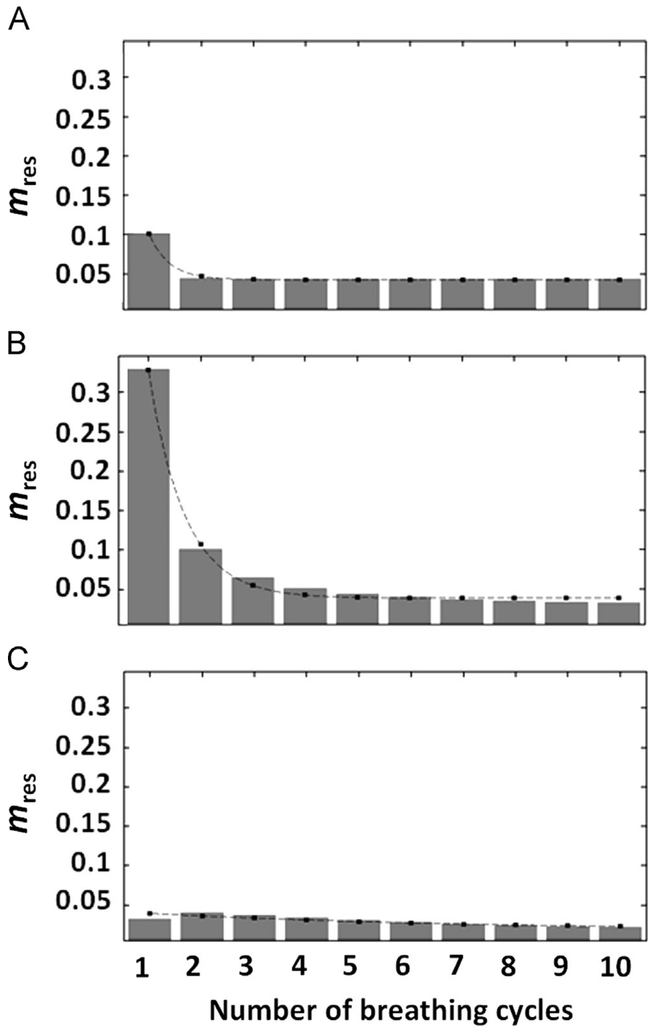

Fig. 8. Washout of the numerical tracer as measured by m_{res} for three values of Q_A/Q_D. Panel A: $Q_A/Q_D = 3 \times 10^{-4}$, Panel B: $Q_A/Q_D = 2.5 \times 10^{-3}$, and Panel C: $Q_A/Q_D = 1.1 \times 10^{-1}$.

Table 3
Exponential fit parameters for expressing m_{res} as a function of the number of washout cycles.

Generation	Q_A/Q_D	m_I	m_T	τ
17	3.037E−04	0.062	0.042	0.387
18	6.162E−04	0.159	0.032	0.435
19	1.266E−03	0.251	0.054	0.572
20	2.689E−03	0.291	0.037	0.694
21	6.134E−03	0.270	0.025	0.744
22	1.655E−02	0.146	0.018	1.050
23	8.568E−02	0.035	0.006	5.276

4. Discussion

A CFD model is presently developed to study convective transport in a single alveolar geometry and most specifically the role of convective mixing resulting from the back and forth fluid motion of air in a rhythmically deformed alveolus. Moreover, by varying the values of the alveolar-to-duct flow ratio Q_A/Q_D in the physiological range observed in the acinus, such a single alveolar model was able to mimic mixing phenomena over the entire acinar region (i.e., generations 17–23) (Soong et al., 1979). Contrary to previous acinar transport studies in which a Lagrangian approach is used (Tsuda et al., 1999, 2008), the Eulerian approach presently proposed enables us to capture the essential of gas flow in the acinar region while minimizing the numerical errors potentially associated to the Lagrangian approach (Tsuda et al., 1995).

We purposely consider a continuous scalar field aiming to describe the probability of finding an average concentration of scalar at a given location in the alveolus. In particular, to assess the efficiency of convective mixing, we calculated the residual quantity of scalar (i.e., an Eulerian fluid marker) m_{res} remaining in the alveolus after one loaded alveolar breathing cycle. Complementarily, the efficiency of mixing was also estimated by imposing a succession of washout maneuvers made of several unloaded breathing cycles. The dispersion of the marker is related to two distinct mechanisms which have been clearly identified in previous studies in more or less similar acinar geometries: flow irreversibility and chaoticity (Haber & Tsuda, 2006; Laine-Pearson & Hydon, 2010). However, as numerical diffusion cannot be completely eliminated, it would be expected that as m_{res} becomes very small after many cycles the proportion of m_{res} due to numerical diffusion, if relatively constant, would be proportionally greater.

We attempt to show herein that the method presently proposed (the Eulerian marker) is particularly adapted to the study of convective acinar mixing at low *Re*. Note that, in our acinar model, irreversibility remains significant in spite of in phase alveolar and airway flows imposed by the homothetic nature of the acinar model deformation. The characteristics of chaotic effects are generated at certain locations (i.e., near the alveolar mouth in some alveoli) and for certain flow conditions where stretching and folding due to shear and expansion are the strongest and convective effects ascertained by non-zero Reynolds number are not negligible. Noteworthy, even this highly simplified alveolar geometry can be used to appropriately simulate alveolar mixing effects.

An important message brought by this quantitative approach is that, in physiological conditions of breathing, convective mixing is maximal in the middle of the acinar region (generations 19–21 of the Weibel and Soong et al. models), i.e., at a place in the range of flow ratio values where the marker dispersion is maximal (Fig. 6). These results are consistent with the results obtained in a computational acinar model by Haber & Tsuda (2006) who found a maximum mixing efficiency located at the level of the 21st generation of the Weibel model.

Based on Fig. 6, three acinar regions for mixing can be identified reflecting values of residual scalar at the end of a loaded breathing cycle:

- A proximal acinar flow region ($Q_A/Q_D < 5 \times 10^{-4}$) where the flow entering the alveolus is relatively minor to the duct flow such that a shear flow is induced and characterized by a recirculation eddy. Hence a small amount of scalar remains at the end of the first inhalation–exhalation cycle while the recirculating eddy traps the bolus dispersed in the alveolus, maintaining a significant part of the bolus in the alveolus (see Fig. 8A).
- An intermediate acinar flow region ($5 \times 10^{-4} < Q_A/Q_D < 5 \times 10^{-2}$) where significant mixing occurs because shear flow and aspiration mechanisms are balanced, leading to maximal convective mixing and maximum washout efficiency (Fig. 8B).
- A distal acinar region ($Q_A/Q_D > 5 \times 10^{-2}$) where the dominant mechanism is a significant ventilation of the alveolar cavity but with a reversible flow pattern, leading to poor convective mixing assessed by the smallest amount of residual scalar at the end of the first cycle (see Fig. 8C).

In general, the present results are consistent with the results in the literature. This suggests that the Eulerian approach presently proposed to quantify mixing irreversibility in lung alveoli is a promising method. It is clearly stated in the literature that irreversibility and chaoticity of flow in the acinar region is actually influenced by two mechanisms: (i) the recirculating flow in the alveolus which is induced by the shear flow within the duct and (ii) the flow pulled into (or pushed out of) the alveolar cavity under the effect of the wall motion (Haber et al., 2000, 2003). To describe the relative contribution of these two mechanisms, authors have used a non-dimensional ratio λ which accounts for the relative contribution of alveolar wall motion and shear contribution raised by the duct flow (Haber et al., 2000):

$$\lambda = \frac{Q_A}{8Q_D}\left(\frac{D_D}{D_A}\right)^3 \tag{10}$$

where D_A and D_D are the characteristic diameters of the alveolus and of the duct respectively. Because the deformation in alveolar model geometry is isotropic, the ratio D_A/D_D remains constant over the breathing cycle and therefore λ is directly proportional to Q_A/Q_D. Hence, the use of flow ratio Q_A/Q_D as a relevant independent parameter linked to the alveolar position within the acinus is consistent with the literature (Haber et al., 2000; Henry et al., 2002, 2009; Tsuda et al., 1999, 2008).

However, potential limitations of the present approach might reside in the simplicity of our alveolar geometry used compared to the complexity of the physiological model. For instance, adjacent alveoli on bronchiolar duct are not one but multiple while upstream and downstream flow conditions may vary. Note that Henry et al. (2002) performed numerical studies with multiple alveoli in a two-dimensional model and found that the flow pattern was similar to that in single alveolus model (Tsuda et al., 1995). Models that incorporate more complex geometries such as multiple alveoli attached at the same axial location (alveolar sleeves) on a bronchiole developed by Darquenne et al. (2009) or arranged in an asymmetric pattern along the bronchiole as studied by Kumar et al. (2009) exhibit some dependence on the relative alveolar position. However, these effects can be taken into account by using an appropriate Q_A/Q_D ratio, i.e., by correcting Q_D to reflect the presence of the adjacent alveoli. Indeed, Kumar and coworkers have specifically shown that alveoli positioned in different acinar structures possess similar flow patterns if Q_A/Q_D values are the same. Regarding upstream and downstream conditions, the entrance length to establish fully developed flow (ℓ) is given by $\ell/D_D = 0.06Re$ for laminar flows, which corresponds within the model to $\ell = 0.03D_D$. Since this length is very small (i.e., smaller than a mesh cell size), the flow is fully established at the inlet boundary of alveoli and does not interfere with the flow in the cavity. Thus, it is unlikely that single isolated alveolus will be highly affected by upstream and downstream conditions.

Foremost, because the model captures the most pertinent local parameters (geometrical size, local flow rates, rate of deformation), the alveolar flow pattern is similar to those found in previous numerical studies (Haber et al., 2003; Henry et al., 2009; Tsuda et al., 2008) despite the lack of phase difference between duct and alveolar flows in our model. The results presented herein can be compared to other numerical studies of alveolar flow presented in the literature (Haber et al., 2000, 2003; Henry et al., 2002, 2009; Kumar et al., 2009; Sznitman et al., 2007; Tsuda et al., 1994a,b, 1999, 2002). To do so, we used data presented in Fig. 6 as an indicator of flow irreversibility then compared them to the findings of other investigators. Consistently with our results, Henry et al. (2002) demonstrated that alveolar flows, in the range 5×10^{-3}–5.3×10^{-3} for Q_A/Q_D, exhibited large recirculation eddies that favor trapping of fluid particles. On the other hand, in the range 4×10^{-2}–7×10^{-2} of Q_A/Q_D, the trajectories of massless particles were not reversible during one breathing cycle while trajectories became completely reversible for Q_A/Q_D values higher than 8×10^{-2}. These range results are also consistent with the results herein.

The investigation of alveolar fluid mechanics needs numerical studies because of the inherent difficulties of performing both in vivo and in vitro experiments (Unglert et al., 2012). In spite of a limited number of in vitro studies conducted to measure velocity flow fields in an expanding/contracting alveolus (Chhabra & Prasad, 2010; Tippe & Tsuda, 2000), these studies have clearly demonstrated the relationship existing between recirculation eddies developing inside the alveolus and the breathing conditions through the role of the Q_A/Q_D ratio. The agreement classically found between numerical and experimental approaches (Berg et al., 2010; Karl et al., 2004; Ma et al., 2009) is a confirmation of the validity and interest of the present approach.

We contend that the present approach using an Eulerian scalar is relevant for our goal of providing a compact analytical expression of flow irreversibility and chaoticity. For future applicative studies, such a compact correlation found between m_{res} and Q_A/Q_D can be used as an input to the existing aerosol deposition model (Pichelin et al., 2012), thus accounting for the effects of flow irreversibility in the context of multiple breathing cycles on aerosol deposition in the acinus. However, in the process of determining the deposition probabilities of aerosols, an inconsistency may arise because our concept is only based on the capture of fluid (i.e., gas) in the alveoli while aerosol particle motion in principle can be independent to the fluid particle motion. This inconsistency is minor for submicron particles which are most likely to reach the acinus and follow the fluid flow ($Stk \ll 1$ and $Pe \ll 1$, in Table 2). Therefore, any approach of particle deposition based on particle residence time in the alveoli could benefit from the present quantification of convective mixing by a non-diffusive Eulerian marker that provides a compact analytical expression of flow irreversibility and chaoticity.

5. Conclusion

Lung convective mixing arising from the irreversibility and chaoticity of flow in the alveoli is an important mechanism of gas and particle transport. Its quantification is classically performed by a Lagrangian approach which is cumbersome and potentially a source of numerical errors. To quantify alveolar convective mixing, we presently show that an Eulerian marker quantifying the amount of fluid particles trapped in an elementary deformable alveolar model can provide a compact analytical expression of alveolar flow irreversibility. The results obtained by such a global marker of alveolar convective dispersion are consistent with the results obtained by the more local Lagrangian approach. For instance, the dependence of the Eulerian marker on alveolar-to-duct flow ratio allows us to infer that optimal efficiency of convective mixing exists in the intermediate region of the acinus for normal breathing conditions. The quantitative results presented in this paper could be a useful tool to incorporate convective alveolar transport and residence time of particles in a model of particle deposition in the lung.

Acknowledgments

For this research, we acknowledge receipt of grants from Agence Nationale de la Recherche: ANR no. 07-TECSAN-005-04 and ANR no. 2010-BLAN-1119-05.

References

Berg, E.J., Weisman, J.L., Oldham, M.J., & Robinson, R.J. (2010). Flow field analysis in a compliant acinus replica model using particle image velocimetry (PIV). *Journal of Biomechanics*, *43*(6), 1039–1047.

Butler, J.P., Oldmixon, E.H., & Hoppin, F.G. (1996). Dihedral angles of septal "bend" structures in lung parenchyma. *Journal of Applied Physiology*, *81*(4), 1800–1806.

Chhabra, S., & Prasad, A.K. (2010). Flow and particle dispersion in a pulmonary alveolus. Part I: Velocity measurements and convective particle transport. *Journal of Biomechanical Engineering—Transactions of the ASME*, *132*(5), 051009.

Darquenne, C., Harrington, L., & Prisk, G.K. (2009). Alveolar duct expansion greatly enhances aerosol deposition: A three-dimensional computational fluid dynamics study. *Philosophical Transactions of the Royal Society A—Mathematical Physical and Engineering Sciences*, *367*(1896), 2333–2346.

Forrest, J.B. (1970). Effect of changes in lung volume on the size and shape of alveoli. *Journal of Physiology—London*, *210*(3), 533–547.

Glatzel, T., Litterst, C., Cupelli, C., Lindemann, T., Moosmann, C., Niekrawietz, R., Streule, W., Zengerle, R., & Koltay, P. (2008). Computational fluid dynamics (CFD) software tools for microfluidic applications—A case study. *Computers & Fluids*, *37*(3), 218–235.
Greaves, I.A., Hildebrandt, J., & Hoppin, F.G., Jr. (1986). *Micromechanics of the lung*. John Wiley & Sons, Inc: .
Haber, S., Butler, J.P., Brenner, H., Emmanuel, I., & Tsuda, A. (2000). Shear flow over a self-similar expanding pulmonary alveolus during rhythmical breathing. *Journal of Fluid Mechanics*, *405*, 243–268.
Haber, S., & Tsuda, A. (2006). A cyclic model for particle motion in the pulmonary acinus. *Journal of Fluid Mechanics*, *567*, 157–184.
Haber, S., Yitzhak, D., & Tsuda, A. (2003). Gravitational deposition in a rhythmically expanding and contracting alveolus. *Journal of Applied Physiology*, *95*, 657–671.
Haefeli-Bleuer, B., & Weibel, E.R. (1988). Morphometry of the human pulmonary acinus. *Anatomical Record*(4), 401–414.
Henry, F.S., Butler, J.P., & Tsuda, A. (2002). Kinematically irreversible acinar flow: A departure from classical dispersive aerosol transport theories. *Journal of Applied Physiology*, *92*, 835–845.
Henry, F.S., Laine-Pearson, F.E., & Tsuda, A. (2009). Hamiltonian chaos in a model alveolus. *Journal of Biomechanical Engineering*, *131*, 011006.
Hinds, W.C. (2014). *Aerosol technology: Properties, behavior, and measurement of airborne particles*. Wiley-Interscience: New York.
Karl, A., Henry, F.S., & Tsuda, A. (2004). Low Reynolds number viscous flow in an alveolated duct. *Journal of Biomechanical Engineering*, *126*, 420–426.
Kitaoka, H., Nieman, G.F., Fujino, Y., Carney, D., DiRocco, J., & Kawase, I. (2007). A 4-dimensional model of the alveolar structure. *Journal of Physiological Sciences*, *57*(3), 175–185.
Kumar, H., Tawhai, M.H., Hoffman, E.A., & Lin, C.-L. (2009). The effects of geometry on airflow in the acinar region of the human lung. *Journal of Biomechanics*, *42*(11), 1635–1642.
Laine-Pearson, F.E., & Hydon, P.E. (2010). Alternating flow in a moving corner. *European Journal of Mechanics B—Fluids*, *29*(4), 278–284.
Lee, D.Y., & Lee, J.W. (2003). Characteristics of particle transport in an expanding or contracting alveolated tube. *Journal of Aerosol Science*, *34*(9), 1193–1215.
Ma, B., Ruwet, V., Corieri, P., Theunissen, R., Riethmuller, M., & Darquenne, C. (2009). CFD simulation and experimental validation of fluid flow and particle transport in a model of alveolated airways. *Journal of Aerosol Science*, *40*(5), 403–414.
Pichelin, M., Caillibotte, G., Katz, I., & Martonen, T.B. (2012). Categorization of lung morphology based on FRC and height: Computer simulations of aerosol deposition. *Aerosol Science and Technology*, *46*(1), 70–81.
Roache, P. (1982). *Computational fluid dynamics*. Hermosa Publishers: Albuquerque, NM, USA.
Soong, T.T., Nicolaides, P., Yu, C.P., & Soong, S.C. (1979). Statistical description of the human tracheobronchial tree geometry. *Respiratory Physiology*, *37*(2), 161–172.
Sznitman, J., Heimsch, F., Heimsch, T., Rusch, D., & Rosgen, T. (2007). Three-dimensional convective alveolar flow induced by rhythmic breathing motion of the pulmonary acinus. *Journal of Biomechanical Engineering*, *129*(5), 658–665.
Sznitman, J., Heimsch, T., Wildhaber, J.H., Tsuda, A., & Rosgen, T. (2009). Respiratory flow phenomena and gravitational deposition in a three-dimensional space-filling model of the pulmonary acinar tree. *Journal of Biomechanical Engineering—Transactions of the ASME*, *131*(3), 031010.
Tippe, A., & Tsuda, A. (2000). Recirculating flow in an expanding alveolar model: Experimental evidence of flow-induced mixing of aerosols in the pulmonary acinus. *Journal of Aerosol Science*, *31*(8), 979–986.
Tsuda, A., Butler, J.P., & Fredberg, J.J. (1994a). Effects of alveolated duct structure on aerosol kinetics. I. Diffusional deposition in the absence of gravity. *Journal of Applied Physiology*, *76*(6), 2497–2509.
Tsuda, A., Butler, J.P., & Fredberg, J.J. (1994b). Effects of alveolated duct structure on aerosol kinetics. II. Gravitational sedimentation and inertial impaction. *Journal of Applied Physiology*, *76*(6), 2510–2516.
Tsuda, A., Henry, F.S., & Butler, J.P. (1995). Chaotic mixing of alveolated duct flow in rhythmically expanding pulmonary acinus. *Journal of Applied Physiology*, *79*(3), 1055–1063.
Tsuda, A., Henry, F.S., & Butler, J.P. (2008). Gas and aerosol mixing in the acinus. *Respiratory Physiology & Neurobiology*, *163*(1–3).
Tsuda, A., Otani, Y., & Butler, J.P. (1999). Acinar flow irreversibility caused by perturbations in reversible alveolar wall motion. *Journal of Applied Physiology*, *86*(3), 977–984.
Tsuda, A., Rogers, R.A., Hydon, P.E., & Butler, J.P. (2002). Chaotic mixing deep in the lung. *Proceedings of the National Academy of Sciences of the United States of America*, *99*(15), 10173–10178.
Unglert, C.I., Namati, E., Warger, W.C., Liu, L., Yoo, H., Kang, D., Bouma, B.E., & Tearney, G.J. (2012). Evaluation of optical reflectance techniques for imaging of alveolar structure. *Journal of Biomedical Optics*, *17*(7), 071303.
Weibel, E.R. (1963). *Morphometry of the human lung*. Springer-Verlag: Berlin.
Weibel, E.R., Sapoval, B., & Filoche, M. (2005). Design of peripheral airways for efficient gas exchange. *Respiration Physiology & Neurobiology*, *148*(1–2), 3–21.